第 41 卷 第 7 期
2020 年 7 月
焊 接 学 报
TRANSACTIONS OF THE CHINA WELDING INSTITUTION
Vol. 41(7):53 − 58
July 2020

填粉率对复合粉粒和实心焊丝堆焊合金组织及耐磨性的影响

龚建勋， 姚惠文， 程诗尧， 刘超， 黄洪江
(湘潭大学, 湘潭, 411105)

摘要: 粉末组分经干混、掺粘结剂湿混、旋转造粒、烧结和筛分等工序制备成 10 目 ~ 30 目的复合粉粒, 将之预置于焊道, 以 H08A 实心焊丝为电弧载体, 自保护明弧堆焊高铬合金. 借助光学显微镜、X 射线衍射仪、扫描电镜等方法, 研究了填粉率对复合粉粒和实心焊丝堆焊合金组织及耐磨性的影响. 结果表明, 随着填粉率由 30% 提高至 45%, 该堆焊合金的显微组织由亚共晶转变为过共晶结构, 主要基体由 γ-Fe 转变为 α-Fe, M_7C_3 相形态由沿晶断续网状或树枝状转变为颗粒状或块状. 磨损试验结果表明, 该方法堆焊的高铬合金耐磨性优良, 与药芯焊丝堆焊高铬合金相当, 制备工艺更为简便且经济, 合金磨损机制包括磨粒的微切削和显微剥落两种形式.

关键词: 复合粉粒; 实心焊丝; 明弧; 堆焊; 高铬合金
中图分类号: TG 422.1 **文献标识码:** A **doi:** 10.12073/j.hjxb.20200429002

0 序言

作为一种经济可靠的方法, 堆焊广泛应用于制造和再制造先进机械零件的耐磨或者耐腐蚀层[1-3]. 常用的堆焊材料主要有: 药皮焊条、药芯焊丝、实心焊丝、焊带以及合金粉块等, 其中药皮焊条因熔敷效率低而逐渐被药芯焊丝所代替[4]. 药芯焊丝组分调整方便, 可适应多种工况, 但需经多道轧辊压制并拉拔减径而成, 制备步骤复杂, 轧辊调整工艺繁琐, 设备维护成本高, 致使药芯焊丝新产品研制及调整周期长, 难以满足焊接生产高效和快速发展的要求[5]. 实心焊丝和焊带因拉拔成形的塑性要求, 可添加碳量极为有限, 仅能制造低合金耐磨或者耐腐蚀零件. 合金粉块作为一种堆焊材料, 由合金粉末掺水玻璃等粘结剂压制而成, 以碳极熔化粉块而制备耐磨合金, 但引弧难、焊缝成形差和熔敷效率偏低. 近年来, 研究表明, 粉末和实心焊丝埋弧焊方法可制备耐磨合金, 但该类合金通常合金量低而呈亚共晶组织[6-9]; 少数几种也可获得过共晶结构, 但填充粉末组合极为特殊, 不具有普遍适用性而难以大范围使用. 该方法的突出意义在于: 通过粉末和实心焊丝组合为填充材料而制备耐磨合金方法具有可行性. 作为主流耐磨合金, 高铬合金的初生 M_7C_3 相或 $M_{23}C_6$ 相对耐磨性起主导作用, 共晶 M_7C_3 等影响合金韧性, 该合金耐磨性和经济性较好, 研究和应用热度依然不减, 且可通过填粉式堆焊法予以制备[10-12]. 综合来看, 堆焊所用药皮焊条或者药芯焊丝均包含两部分: H08A 钢+合金粉末, 只是分布位置相反. 鉴于此, 文献 [13] 提出了“复合粉粒”的概念及其制备工艺, 这是一种经称量干混、掺粘结剂湿混、旋转造粒、烧结和筛分等工序而成的新型焊接材料. 与药芯焊丝和药皮焊条相比, 该复合粉粒的制备工艺显著简化, 生产周期短, 可适应焊接生产快速的发展要求. 文中在文献 [13] 所述复合粉粒制备工艺的基础上, 研究复合粉粒占填充材料的重量百分比, 即填粉率对复合粉粒和 H08A 实心焊丝堆焊高铬合金的性能影响.

1 试验方法

1.1 复合粉粒制备

复合粉粒包含高碳铬铁 (70% Cr, 8% C, 质量分数, 下同)、钒铁 (50% V)、钛铁 (30% Ti)、鳞片石墨 (98% C 以上) 以及还原铁粉等粉末. 所有粉末组分先过 60 目筛, 再经称量干混、掺入水玻璃湿混、旋转造粒、烧结和筛分等工序, 获得 10 目 ~ 30 目

收稿日期: 2020 − 04 − 29
基金项目: 湖南自然科学基金资助项目 (2015JJ5031)

的复合粉粒, 工艺参数同文献 [13] 所述.

1.2 电弧堆焊高铬合金

在 160 mm × 75 mm × 16 mm 的 Q235A 为基体的钢板上, 先将复合粉粒均匀预置于焊道表面, 采用 ZD5-1000E 直流焊机进行自保护明弧焊, 工艺参数如表 1 所示. 以 ϕ2.5 mm 的 H08A 实心焊丝作为电弧载体, 使预置复合粉粒熔化, 与实心焊丝熔化熔滴熔合为一体化堆焊熔体, 空冷凝固.

表 1 堆焊工艺参数

Table 1 Hardfacing experiment parameters

电流I/A	电压U/V	焊丝伸出长度L/mm	焊接速度v/(mm·s^{-1})	层温T/℃	焊后状态	极性
410	27	30	4.5	100 ~ 150以下	空冷	反接

填粉率 = 复合粉粒/(实心焊丝 + 复合粉粒), 即复合粉粒占焊接填充材料的质量分数. 用精度 0.001 g 的 KFS-C8 型电子天平焊接前后分别测试堆焊试样和实心焊丝的重量, 计算其重量差, 即可获得填粉率. 改变填粉率, 制备如表 2 所示的 1 号 ~ 5 号试样.

表 2 堆焊合金的填粉率 (质量分数, %)

Table 2 Powder addition ratios of hardfacing alloys

1号	2号	3号	4号	5号
30	33	38	42	45

1.3 组织表征与性能测试

用 HFX-ⅡA 型尼康金相显微镜、JSM-6360LV 扫描电镜观察试样的组织形貌; D/MAX2550VB 型 X-射线衍射仪对未腐蚀的块状金相试样分析相组成, 结合 Oxford7854 能谱仪对试样微区成分扫描鉴定具体物相.

采用 HR-150A 型洛氏硬度计测试堆焊层表面宏观硬度, 加载 1 470 N, 保持 15 s. 使用 HV-1000 型显微硬度计沿堆焊层厚度方向测定其截面的显微硬度分布, 载荷为 1.96 N, 保持 10 s.

线切割制备尺寸 57 mm × 25.5 mm × 6 mm 的磨损试样, 在 MLS-225 型湿砂橡胶轮式磨损试验机进行耐磨性试验, 以磨损失重 ΔM 评估试样耐磨性, JSM-6360LV 扫描电镜观察其磨损形貌.

2 结果与讨论

2.1 高铬堆焊合金的相组成

图 1 为 1 号和 5 号试样的相组成, 该堆焊试样的填粉率分别为 30% 和 45%. 由图可知, 1 号堆焊合金基体主要为 γ-Fe, 还有少量的 α-Fe, 硬质相有 M_7C_3、(Ti,V)C 等; 5 号堆焊合金的基体由 α-Fe 和 γ-Fe 组成, 其中 α-Fe 为主要基体, 硬质相包含 M_7C_3, (Ti,V)C, M_3C 等. 由此可知, 随着填粉率提高, 堆焊合金所含合金化元素量上升, γ-Fe 基体发生转变, 即有: γ-Fe → α-Fe + (Ti,V)C + M_7C_3 + M_3C. 此外, 5 号试样 M_7C_3 的 (420) 面特征峰 (d=2.30Å) 明显增强, 说明其 M_7C_3 相数量显著增加, 这有利于改善该方法堆焊合金的耐磨性.

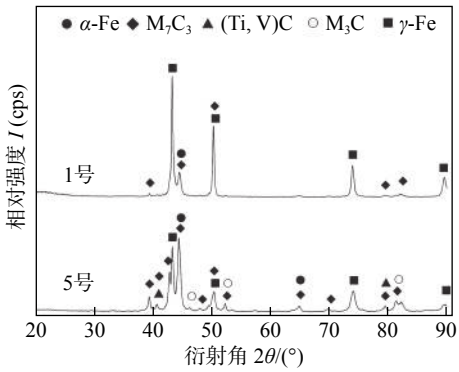

图 1 高铬堆焊合金的 XRD 谱

Fig. 1 XRD of high chromium hardfacing alloys

图 2 为复合粉粒和实心焊丝堆焊高铬合金的显微组织. 结合图 1 所示 XRD 谱, 可知图 2a 所示白色胞状体为 γ-Fe 相, 沿该胞状相晶界呈断续网状或者树枝状的灰色相为沿晶 M_7C_3 相, 其中含有少量的 α-Fe. 图 2c 显示, 填粉率增加时, 白色胞状 γ-Fe 相尺寸减小, 沿晶 M_7C_3 数量显著增加. 图 2d 所示 M_7C_3 型碳化物呈颗粒状, 其中还有灰色的团状体, 应为石墨裂解所形成的高碳区. 图 2e 显示其中出现白色的块状相, 测试显示该白色块状相显微硬度均值为 1 170 HV, 可知其为初生 M_7C_3 相. 图 2f 所示板条状白色组织为初生 M_7C_3 相. 对比图 2a ~ 图 2f 可知, 随着填粉率增加, 焊接材料所含复合粉粒的重量比例增大, 堆焊合金的碳及碳化物形成元素如 Cr, V 含量提升, 组织由亚共晶先转变为共晶, 再转变为过共晶结构; M_7C_3 相由沿晶碳

化物逐渐转变块状初生相，形态从断续网状或者树枝状改变为颗粒状，然后转变为块状或者板条状．此外，原位析出 (Ti,V)C 型碳化物，因其中的合金化元素 V，Ti 对碳的亲和力远大于 Cr，Fe，可优先析出，阻断沿晶碳化物的网状连续性，使之呈断续网状，降低该沿晶碳化物的刚性而降低合金脆性．不仅如此，少量固溶于初生 M_7C_3 相的强碳碳化物形成元素 V，使堆焊熔体高碳团簇先期形成而促进 M_7C_3 优先析出．以上结果表明，填粉率显著影响复合粉粒和实心焊丝堆焊合金的显微组织及相组成．

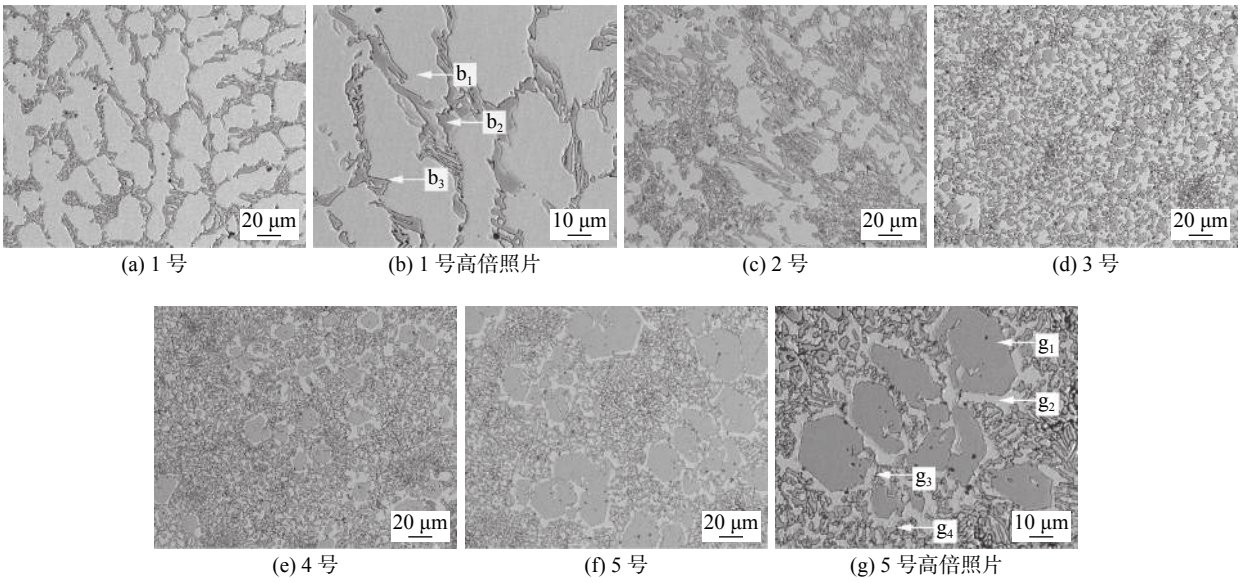

(a) 1 号　(b) 1 号高倍照片　(c) 2 号　(d) 3 号

(e) 4 号　(f) 5 号　(g) 5 号高倍照片

图 2　高铬堆焊合金的显微组织

Fig. 2　Microstructure of high chromium hardfacing alloys. (a, b) No.1; (c) No.2; (d) No.3; (e) No.4; (f, g) No.5

对图 2b 和图 2g 的微区进行 EDS 成分扫描，结果列于表 3．对比图 2a、图 2c、图 2d、图 2e 和图 2f 可知，随着填粉率提高，堆焊合金的碳化物数量增加，体积分数不断增大，形态由断续网状或者树枝状转为颗粒状、块状分布．

由表 3，并结合图 1 所示 XRD 谱的相组成结果可知，图 2b 所示胞状微区 b_1 组织为奥氏体，微区 b_2 相的成分显示其中 Cr，V 元素含量高，应为断续网状或者树枝状的沿晶 M_7C_3 相．另外，微区 b_3 处的 Ti，V 含量较高而图 3b 显示其中有少量黑色点状相，结合图 1 结果以及原位析出相的形态分析可知，该处有原位析出的 (Ti,V)C 型碳化物．

表 3　高铬堆焊合金的微区化学成分 (原子分数，%)

Table 3　Micro-area chemical composition in high chromium hardfacing alloys

能谱点	C	Ti	V	Cr
b_1	20.78	—	0.52	7.32
b_2	36.95	—	4.17	26.66
b_3	20.89	9.13	8.33	26.44
g_1	28.42	0.11	4.09	36.11
g_2	14.66	0.13	0.57	10.39
g_3	16.86	37.03	16.52	10.12
g_4	22.32	0.22	2.75	25.00

图 2g 所示微区 g_1 的白色块状相的 Cr，V 含量高，该相为初生 M_7C_3 相，即为 $(Cr,Fe,V)_7C_3$ 相，其中 Cr 和 V 含量明显高于传统初生 M_7C_3 相．这说明该组织形核生长机制与传统药芯焊丝所制备的高铬堆焊合金有所不同，有待进一步研究．微区 g_2 处铬含量较高，但碳含量低于 b_1 处，应该为富铬铁素体基体或者奥氏体；微区 g_3 处的 V 与 Ti 含量，该处为黑色块状，为原位析出的 (Ti,V)C 相；微区 g_4 处的 C，V，Cr 含量均低于 g_1 处，但其碳含量高于 g_3 处，为二次 M_7C_3 相或者 M_3C 相．

由图 2 的碳化物形态可知，高铬堆焊合金的沿晶 M_7C_3 型碳化物呈长条状或者颗粒状，未出现蜂窝状的脆性莱氏体结构．随着填粉率提高，共晶或者二次 M_7C_3 型碳化物多呈颗粒状或者块状弥散分布；上述碳化物形态均不同于药芯焊丝堆焊高铬合金，说明采用复合粉粒作为焊接填充材料，可有效改善堆焊合金的碳化物形态，有利于增强合金韧性．

2.2　高铬堆焊合金的性能

图 3 为 1 号和 5 号高铬合金堆焊层横截面的显微硬度分布曲线．由此可知，1 号高铬堆焊合金

层的显微硬度分布均匀，硬度波动值小，这说明截面组织较为均匀；5 号试样堆焊层从熔合区到最表层的显微硬度值波动较大，这与组织改变过大有关. 由于 Q235A 基体的合金元素量显著低于高铬合金层，因而对紧靠熔合区处的焊缝组织具有较大的成分稀释效应[14]. 5 号试样堆焊层表面最高硬度约为基体硬度的 4 倍，焊缝中部硬度略低，受母材成分稀释的影响而析出尺寸偏小的弥散 M_7C_3 相；临近最表层区域硬度最高，主要在于该处初生 M_7C_3 相呈块状或者板条状，硬度值已达 878 ~ 956 HV，接近碳化物本身的显微硬度，说明该处碳化物等硬质相体积分数高；最表层硬度下降，其主要原因是由于该处冷却快，所形成的初生 M_7C_3 相尺度较之偏小所致.

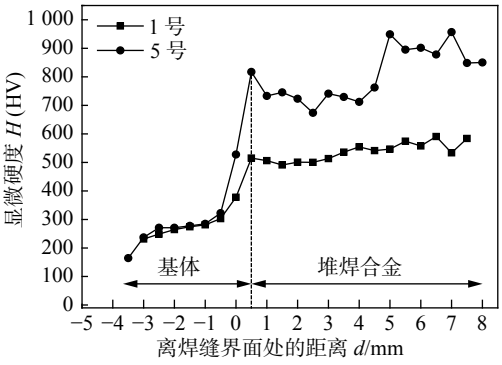

图 3 试样 1 号和 5 号堆焊合金层横截面的显微硬度曲线

Fig. 3 Micro-hardness curves of cross-sections of No.1 and No.5 hardfacing alloy layers

图 4 为填粉率对复合粉粒和实心焊丝堆焊高铬合金的宏观硬度和磨损失重的影响. 由此可知，随着填粉率增加，高铬堆焊合金的宏观硬度随之呈正比上升，但磨损失重先显著下降，然后小幅下降，最后稍有上升.

1 号试样的硬度值最低为 38.3 HRC，这主要与其含有数量较多的奥氏体有关；随填粉率提高，堆焊合金的碳化物体积分数增加，且尺寸增加，其宏观硬度提高至 5 号试样的 58.1 HRC，这与药芯焊丝高铬堆焊合金的硬度相当. 5 号试样的填粉率为 45%，与药芯焊丝通常 43% ~ 52% 的填充率相当. 填粉率 42% 时，复合粉粒和实心焊丝堆焊高铬合金的磨损失重最小，仅为 1.988 mg，耐磨性是 1 号试样的 16.4 倍，这说明填粉率显著影响复合粉粒和实心焊丝堆焊高铬合金的耐磨性. 4 号和 5 号试样的磨损失重与药芯焊丝高铬堆焊合金相当[15]，这说明以复合粉粒和实心焊丝自保护明弧堆焊法而制

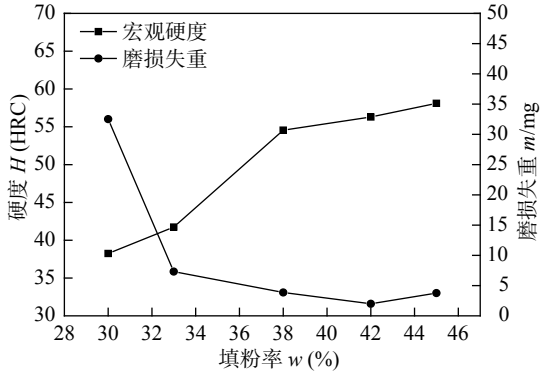

图 4 填粉率对高铬堆焊合金的宏观硬度和磨损失重的影响

Fig. 4 The effects of powder addition ratio on the macro-hardness and wear mass loss of high-chromium hardfacing alloys

备高铬合金的方法完全可行，该合金耐磨性已达到药芯焊丝高铬合金的同类水准，但该方法更为简便且经济，制备周期极短，可适应焊接生产快速的发展要求.

图 5 为高铬堆焊合金的磨损形貌. 图 5a 显示 1 号试样的划痕较多，且呈直线走向，这说明磨粒的显微切削运动没有受到阻碍，其原因主要与奥氏体基体有关；胞状奥氏体偏软，非常有利于磨粒锲入，而其周围沿晶碳化物对磨粒显微切削运动阻碍小，因而磨损失重大. 与 1 号试样相比，图 5b 所示 4 号试样的划痕数量明显偏少，这主要与其碳化物的数量增加有关；图 5c 显示该 5 号试样的划痕不明显，但出现了剥落坑. 对照图 2f 可知，这些剥落坑主要位于共晶组织区. 由于共晶组织脆性大，在外加冲击和磨粒碾压作用易开裂而剥落，这导致其磨损失重较 4 号试样稍微增大. 对比图 2e 和图 2f 可知，尽管 4 号试样的主耐磨相 M_7C_3 体积分数和尺寸均明显低于 5 号试样，但其共晶碳化物尺寸明显偏小，且具有一定数量的塑性奥氏体，这可缓冲外加冲击作用，提高该共晶组织区的韧性，而 5 号试样共晶区基本为变态共晶，其共晶碳化物尺寸偏大则易萌生裂纹，形成剥落坑而加大磨损.

由图 5 所示高铬堆焊合金的磨损形貌可知，其表面磨损为磨粒磨损，磨损机制为微切削和显微剥落磨损两种机理，先以微切削形式为主，随填粉粒提高，转变显微剥落形式为主.

2.3 复合粉粒的作用

通常粉末堆焊均采用混合粉末或者复合粉末进行作业，其中混合粉末中的碳组分如石墨，极易在电弧吹力作用下严重流失，仅可得到亚共晶结构

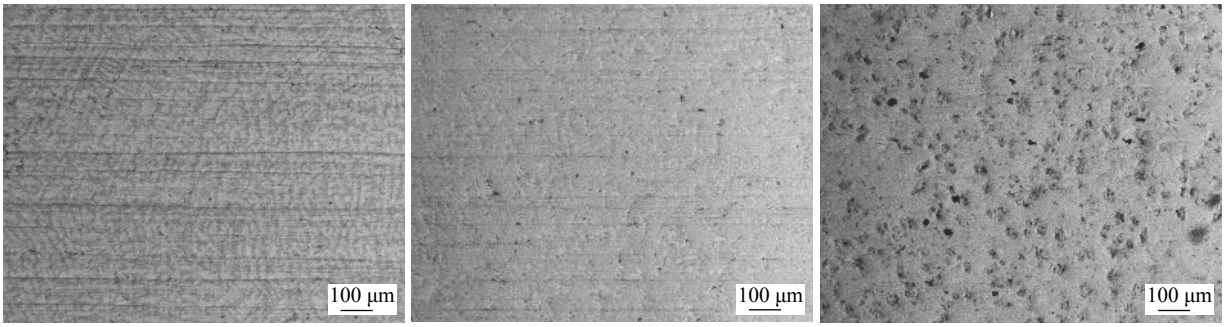

(a) 1 号　(b) 4 号　(c) 5 号

图 5　高铬堆焊合金的磨损形貌

Fig. 5　Worn morphology of high chromium hardfacing alloys. (a) No.1; (b) No.4; (c) No.5

的堆焊合金. 鉴于此，若将之做成重量大的复合粉末，则需将所有组分加热熔化为液态金属，然后吹成粉末，制备工艺复杂，这导致可供的复合粉末种类极为有限. 文中所采用的复合粉粒经由称量干混、掺粘结剂湿混、旋转造粒、烧结和筛分等工序制备而成，堆焊之前将复合粉粒置于焊道上，之后在电弧作用下与实心焊丝共同熔化形成一体化堆焊熔池，凝固形成焊缝，制备工艺简单快速.

为了阐明复合粉粒的作用效果，将 5 号试样的粉末组分，一种直接做成混合粉末，另外一种掺入粘结剂制成复合粉粒，然后二者在同一工艺参数进行自保护明弧堆焊，这两种堆焊合金与 Q235A 界面处的显微组织如图 6 所示.

图 6a 所示该混合粉末堆焊合金界面处的组织为典型的亚共晶，表层也如此，这说明该混合粉末中可过渡到熔敷焊缝的合金化元素量少；图 6b 显示复合粉粒堆焊合金界面处基本为过共晶组织，析出数量较多弥散的块状 M_7C_3 型碳化物. 这表明，以复合粉粒作为填充材料，其堆焊合金层受母材的稀释作用比同样组分的混合粉末，要明显减小.

试验采用自保护明弧焊法，以混合粉末进行作业时，合金粉末飞溅量大，焊缝易出现蜂窝状气孔. 但是，当粉末组分制备重量大的复合粉粒，不仅可显著减少飞溅量，而且掺入的粘结剂如水玻璃等化合物，发射电子的逸出功低，具有活性剂的作用；直流反接时，可诱导电弧直接作用于复合粉粒而使之优先熔化，并减小母材的稀释作用. 与混合粉末堆焊法相比，复合粉粒堆焊合金的碳化物数量更多，耐磨性优良，性价比突出.

综上所述，以复合粉粒作为焊接材料，避免了药芯焊丝较为繁琐的轧制成型和拉拔减径等工艺，易获得耐磨性优异的堆焊合金，可实现自动化和连续化堆焊作业. 所制备的耐磨合金性能和组织调整极为便利，成形快且经济，具有明显优势和研究价值.

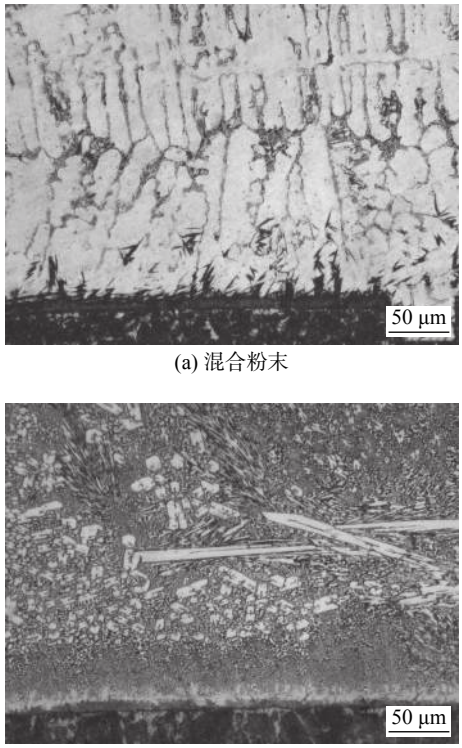

(a) 混合粉末

(b) 复合粉粒

图 6　堆焊合金与基体界面处的组织

Fig. 6　Interface microstructure between hardfacing alloys and base metals. (a) mixed powder; (b) composite powder particles

3　结论

(1) 以复合粉粒和 H08A 实心焊丝自保护明弧焊可制备过共晶结构的高铬合金，其耐磨性和药芯焊丝堆焊高铬合金相当，性能和组织调整极为便利，成形快且经济，性价比突出，在生产作业中有着明显优势和研究价值.

(2) 复合粉粒和 H08A 实心焊丝堆焊高铬合金，随着填粉率提高，合金组织由亚共晶转变为过

共晶结构，基体由 γ-Fe 转变为 α-Fe，M_7C_3 形态从断续网状或者转变为到粒状、块状和板条状.

(3) 随着填粉率的增加，复合粉粒和 H08A 实心焊丝堆焊高铬合金硬度随之呈正比例提高，合金耐磨性先大幅提高，随后小幅下降. 该合金的磨损机制包括微切削和显微剥落磨损两种形式.

参考文献

[1] Correa E O, Alcantara N G, Tecco D G, *et al*. The relationship between the microstructure and abrasive resistance of a hardfacing alloy in the Fe-Cr-C-Nb-V system[J]. Metallurgical and Materials Transactions A, 2007, 38(8): 1671 − 1780.

[2] 魏建军, 潘健, 黄智泉, 等. 耐磨堆焊材料在我国水泥工业中的应用 [J]. 中国表面工程, 2006, 19(3): 9 − 13.
Wei Jianjun, Pan Jian, Huang Zhiquan, *et al*. The application of hardfacing material in Chinese cement industry[J]. China Surface Engineering, 2006, 19(3): 9 − 13.

[3] Lin Yuchi, Chen Hanming, Chen Yongchwang. Microstructures and wear properties of various clad layers of the Fe-W-C-B-Cr system[J]. Surface & Coatings Technology, 2013, 236: 410 − 419.

[4] 刘跃, 张国赏, 魏世忠, 等. 堆焊工艺对高铬合金粉体堆焊层组织及耐磨性能的影响 [J]. 机械工程材料, 2013, 37(8): 27 − 30.
Liu Yue, Zhang Guoshang, Wei Shizhong, *et al*. Effects of surfacing technologies on microstructure and wear resistance of high chromium alloy powder surfacing layer[J]. Materials for Mechanical Engineering, 2013, 37(8): 27 − 30.

[5] 刘大双, 刘仁培, 邱悦. 无渣含铌自保护堆焊药芯焊丝的研制 [J]. 焊接学报, 2012, 33(9): 73 − 76.
Liu Dashuang, Liu Renpei, Qiu Yue. Development of slag-free self-shielded flux cored wire with niobium addition for hardfacing[J]. Transactions of the China Welding Institution, 2012, 33(9): 73 − 76.

[6] Srikarun B, Muangjunburee P. The effect of iron-based hardfacing with chromium powder addition onto low carbon steel[J]. Materials Today: Proceedings, 2018, 5: 9272 − 9280.

[7] 王智慧, 贺定勇, 张杰哲, 等. 用填粉式堆焊方法制造耐磨复合钢板 [J]. 机械工程材料, 2001, 25(3): 25 − 27.
Wang Zhihui, He Dingyong, Zhang Jiezhe, *et al*. The development of wear resistant composite plate with powder adding welding method[J]. Materials for Mechanical Engineering, 2001, 25(3): 25 − 27.

[8] Zahiri R, Sundaramoorthy R, Lysz P, *et al*. Hardfacing using ferro-alloy powder mixtures by submerged arc welding[J]. Surface & Coatings Technology, 2014, 260: 220 − 229.

[9] Yüksel N, Sahin S. Wear behavior-hardness-microstructure relation of Fe-Cr-C and Fe-Cr-C-B based hardfacing alloys[J]. Materials and Design, 2014, 58: 491 − 498.

[10] Coronado J. Effect of $(Fe,Cr)_7C_3$, carbide orientation on abrasion wear resistance and fracture toughness[J]. Wear, 2011, 270(3): 287 − 293.

[11] Günther K, Bergmann J P, Suchodoll D. Hot wire-assisted gas metal arc welding of hypereutectic FeCrC hardfacing alloys: microstructure and wear properties[J]. Surface & Coatings Technology, 2017, 334: 420 − 428.

[12] Li Meiyan, Wang Yong, Han Bin, *et al*. Microstructure and properties of high chrome steel roller after laser surface melting[J]. Applied Surface Science, 2009, 255: 7574 − 7579.

[13] 龚建勋, 程诗尧, 姚惠文, 等. 以复合粉粒和实心焊丝为堆焊材料制备高硼合金的方法: 中国, 201811380791.X[P]. 2019-02-01.
Gong Jianxun, Cheng Shiyao, Yao Huiwen. *et al*. A method forthe preparation of high boron hardfacing alloys with composite powder particles and solid wire: China, 201811380791.X[P]. 2019-02-01.

[14] Miná, Emerson Mendonça, Da Silva Y C, *et al*. Effect of dilution on the microstructure of AWS ERNiCrMo-14 alloy in overlay welding by the TIG process with cold wire feed[J]. Welding International, 2017, 32(2): 130 − 138.

[15] 龚建勋, 肖逸锋, 张清辉, 等. Fe-C-Cr-V 高铬堆焊合金的 M_7C_3 型碳化物及其耐磨性 [J]. 焊接学报, 2010, 31(1): 33 − 36.
Gong Jianxun, Xiao Yifeng, Zhang Qinhui, *et al*. M_7C_3-type carbide and abrasion resistance of Fe-C-Cr-V high chromium hardfacing alloys[J]. Transactions of the China Welding Institution, 2010, 31(1): 33 − 36.

第一作者简介：龚建勋，1973 年出生，博士，副教授；从事电弧增材制造工艺及焊接材料方向的科研和教学工作；发表论文 50 余篇；Email：gong309@tom. com.

（编辑： 张宏强）

Key words: single crystal superalloy; brazing gap; holding time; stress rupture property

Microstructure investigation and residual stress numerical simulation on welded joint of 304/Q345R composite plate

HU Xiaodong[1], WANG Jitao[1], YANG Yicheng[1], SONG Ming[2], QI Pengfei[1] (1. Shandong University of Science and Technology, Qingdao, 266590, China; 2. China University of Petroleum (East China), Qingdao, 266580, China). pp 39-45

Abstract: In order to study the complex thermo-mechanical behavior of the composite plate in the welding process, a finite element model was developed to simulate the welding process of 304/Q345R composite plate. The thermal cycle curve and residual stress distribution of the welded joint were obtained by thermocouple and blind hole method. The finite element model was verified by the experimental results. Meanwhile, the microstructure, grain morphology and element distribution of the welded joint were analyzed by means of optical microscope and scanning electron microscope, and the microstructure evolution of the welded joint was investigated. The results showed that the maximum welding residual stress was 312 MPa, which was located at the weld toe, and the residual stress gradually decreased and stabilized along the direction from the weld to the base metal. At the interface of the two materials, the residual stress discontinuity was observed. The microstructure of the welded joint was composed of austenite and ferrite. The ferrite in the vicinity of the fusion line of the composite layer presents strip and needle-like shape and forms a banded transition zone, while the austenite grains in the vicinity of the fusion line presents columnar morphology and smaller size.

Key words: composite plate; element dilution; microstructure; finite element method; welding residual stress

Effect of Ga_2O_3 on of microstructure and properties of brazed joints obtained by Ag30CuZnSn flux cored brazing filler metal and brass

PU Juan[1,2], XUE Songbai[1], WU Mingfang[2], LONG Weimin[3], WANG Shuiqing[4], LIN Tiesong[5] (1. Nanjing University of Aeronautics and Astronautics, Nanjing, 210016, China; 2. College of Materials Science and Engineering, Jiangsu University of Science and Technology, Zhenjiang, 212003, China; 3. China Innovation Academy of Intelligent Equipment Co., Ltd, Ningbo, 315700, China; 4. Zhejiang Xinrui Welding Technology Co., Ltd, Shaoxing, 312400, China; 5. Harbin Institute of Technology, Harbin, 150001, China). pp 46-52

Abstract: The effect of Ga_2O_3 on the microstructure and properties of brazed joints formed by Ag30CuZnSn flux cored brazing filler metal brazed brass was studied when adding Ga_2O_3 into flux cored brazing powders. The results showed that the micro amount of Ga_2O_3 additions can significantly improve the wettability of Ag30CuZnSn flux cored brazing filler metal and reduce the flux additions. When the content of Ga_2O_3 was 0.4 %, the wettability of Ag30CuZnSn flux cored brazing filler metal and the shear strength of brazed joint was up to the optimum. This was attributed to the fact that Ga_2O_3 was a surfactant, which can significantly reduce the interfacial tension between the molten brazing filler metal and the base metal, to improve the effect of removing oxide film of flux powders. Finally, the wettability of Ag30CuZnSn flux cored brazing filler metal was improved. In the process of flame brazing, when Ga_2O_3 addition was 0.4 %, the shear strength of brazed joint was increased by more than 11% owing to the microstructure refinement of brazing seam and the increase of brazed rate (the brazed rate was increased to more than 95%). The fracture morphology of the brazed joint proved the above results.

Key words: Ga_2O_3; Ag30CuZnSn; flux cored brazing filler metal; wettability; microstructure; shear strength

Effect of powder addition ratio on the microstructure and abrasive wear resistance of hardfacing alloys deposited by composite powder particles and solid wire

GONG Jianxun, YAO Huiwen, CHENG Shiyao, LIU Chao, HUANG Hongjiang (Xiangtan University, Xiangtan, 411105, China). pp 53-58

Abstract: Composite powder particles with the size of 10-30 mesh were prepared by a series of processes including dry mixing, wet mixing with the addition of binding admixture, rotary pelleting, sintering and screen sizing on powder components. Those composite particles presetting on base metals were used as welding consumable together with solid wire which can be considered as arc carrier. High chromium alloys were deposited by the method of self-shielded open arc welding. The effects of powder addition ratio on the microstructure and abrasion resistance were investigated by

optical microscopy (OM), X-ray diffraction (XRD) and scanning electron microscopy (SEM). The results indicate that, with powder addition ratio increases from 30% to 45%, the microstructure changes from the hypoeutectic to the hypereutectic. The dominant matrix converts changes from γ-Fe to α-Fe and the morphology of M_7C_3-type carbides transits from inter-granular reticular or dendritic shapes to granular or block-like ones. The results of wear test show that their abrasion resistance is excellent and corresponds to the one of flux-cored wire hardfacing alloys with such processing merits as simple and economic. The wear mechanism mode of hardfacing alloys includes micro-cutting and micro-spalling.

Key words: composite powder particles; solid wire; open arc; hardfacing; high-chromium alloys

Welding deviation measurement method based on welding torch contour feature extraction WANG Zhongren[1], WANG Xiaogang[1,2], LIU Dezheng[1], LIU Haisheng[1]
(1. Hubei University of Arts & Science, Xiangyang, 441053, China; 2. Wuhan University of Science and Technology, Hubei, 430081, China). pp 59-64

Abstract: In the welding process of gas metal welding (GMAW), due to the serious arc interference, it is difficult for the vision system to accurately extract the weld and the wire tip at the same time, thus affecting the accuracy of the weld tracking. An approach was proposed to locate the welding torch center instead of the welding wire tip. The feasibility of the method was demonstrated. First, after enhancing the weld seam and weld gun edge contour information in the molten pool image, a rectangular window was set to obtain the edge sampling point. Then, the clustering algorithm was used to screen out the correct edge sampling points. The weld line and the ellipse equation of the torch were fitted by the least squares method according to the sampling points. Moreover, the distance between the center of the current image welding torch and the straight line of the weld was calculated. Compared with the corresponding distance in the reference image, the amount of deviation of the welding torch position and the deviation of the welding gun swing were detected. The actual verification results show that the replacement error between the center of the welding torch and the tip of the welding wire is within 0.2 mm, which meets the requirements of tracking accuracy and has strong engineering practical significance.

Key words: weld seam tracking; welding molten pool image; welding deviation; clustering algorithm; gas metal arc welding

Parameter optimization of laser cladding ceramic repair layer of H13 steel LIU Lijun[1,2], LIU Dayu[1], WANG Xiaolu[1], LI Jiqiang[2], CUI Yuanbiao[3], JIA Zhixin[2] (1. Harbin University of Science and Technology, Harbin, 150080, China; 2. Ningbo Institute of Technology, Zhejiang University, Ningbo, 315100, China; 3. Harbin Vocational & Technical College, Harbin, 150081, China). pp 65-70

Abstract: In view of surface problems such as wear and corrosion caused by the failure of H13 die steel, nickel-based silicon carbide powder was used to optimize the parameters of the repair layer of H13 die steel. In order to explore the effect of laser parameters on the repair layer in laser cladding, laser cladding experiments were carried out using different laser currents and defocus amounts as optimized process parameters. It was found that changing the size of the laser current and the amount of defocusing had different degrees of influence on the cladding size, microstructure and mechanical properties of the repair layer. The geometric dilution rate of the cladding layer increases as the laser current increases, and the grain size of the cladding layer becomes coarse; The geometric dilution rate of the cladding layer decreases as the amount of defocus increases, and the grain size of the cladding layer becomes finer. The optimized results obtained through the analysis of metallographic microscope, SEM and micro hardness tester showed that the laser current is 115A, the defocus amount is 51mm, and the microhardness value of the cladding layer reaches the highest value, which is about 2.6 times the hardness of the substrate. The above research results provide theoretical and technical basis for improving the quality of the laser cladding repair layer on the failure surface of the mold.

Key words: laser cladding; grain; repair layer; micro-hardness

Microstructure and microhardness analysis of laser welded dissimilar steel YIN Yan[1], KANG Ping[1], LU Chao[2], ZHANG Yuan[1], ZHANG Ruihua[2,3] (1. State Key Laboratory of Advanced Processing and Recycling of Nonferrous Metals, Lanzhou University of Technology, Lanzhou, 730050, China;